



Terahertz electron paramagnetic resonance spectroscopy using continuous-wave frequency-tunable photomixers based on photoconductive antennae

Ohmichi, Eiji
Fujimoto, Tatsuya
Minato, Keisuke
Ohta, Hitoshi

(Citation)

Applied Physics Letters, 116(5):051101-051101

(Issue Date)

2020-02-03

(Resource Type)

journal article

(Version)

Version of Record

(Rights)

© 2020 Author(s). This article may be downloaded for personal use only. Any other use requires prior permission of the author and AIP Publishing. The following article appeared in Applied Physics Letters 116(5), 051101 and may be found at <http://dx.doi.org/10.1063/1.5133414>

(URL)


<https://hdl.handle.net/20.500.14094/90007107>



Terahertz electron paramagnetic resonance spectroscopy using continuous-wave frequency-tunable photomixers based on photoconductive antennae

Cite as: Appl. Phys. Lett. **116**, 051101 (2020); <https://doi.org/10.1063/1.5133414>

Submitted: 23 October 2019 . Accepted: 11 January 2020 . Published Online: 03 February 2020

Eiji Ohmichi , Tatsuya Fujimoto, Keisuke Minato, and Hitoshi Ohta



View Online



Export Citation



CrossMark

ARTICLES YOU MAY BE INTERESTED IN

[Guest Editorial: The dawn of gallium oxide microelectronics](#)

Applied Physics Letters **112**, 060401 (2018); <https://doi.org/10.1063/1.5017845>

[Nonlinear terahertz emission in the three-dimensional topological insulator Bi₂Te₃ by terahertz emission spectroscopy](#)

Applied Physics Letters **115**, 191102 (2019); <https://doi.org/10.1063/1.5097335>

[Investigation of carrier localization in InAs/AlSb type-II superlattice material system](#)

Applied Physics Letters **115**, 211601 (2019); <https://doi.org/10.1063/1.5127198>

Lock-in Amplifiers
Find out more today



 Zurich Instruments

Terahertz electron paramagnetic resonance spectroscopy using continuous-wave frequency-tunable photomixers based on photoconductive antennae

Cite as: Appl. Phys. Lett. **116**, 051101 (2020); doi: [10.1063/1.5133414](https://doi.org/10.1063/1.5133414)

Submitted: 23 October 2019 · Accepted: 11 January 2020 ·

Published Online: 3 February 2020



View Online



Export Citation



CrossMark

Eiji Ohmichi,^{1,a)}  Tatsuya Fujimoto,¹ Keisuke Minato,¹ and Hitoshi Ohta²

AFFILIATIONS

¹Graduate School of Science, Kobe University, 1-1 Rokkodai, Nada, Kobe 657-8501, Japan

²Molecular Photoscience Research Center, Kobe University, 1-1 Rokkodai, Nada, Kobe 657-8501, Japan

^{a)}ohmichi@harbor.kobe-u.ac.jp

ABSTRACT

In this article, we demonstrate terahertz (THz) electron paramagnetic resonance (EPR) spectroscopy using a frequency-tunable photomixing source/detection system to investigate the electronic structure of solid-state samples in a microscopic manner. Fiber-coupled photoconductive antennae were used to generate and detect continuous THz waves obtained as the beat signals from two laser beams with different wavelengths. We will show some examples of EPR spectroscopy obtained by multi-frequency EPR measurements at room temperature. The technique reported here has several advantages, including high spectral resolution, wide frequency-range operation, high dynamic range, owing to the continuous-wave (cw) and tunable generation/detection of THz waves.

Published under license by AIP Publishing. <https://doi.org/10.1063/1.5133414>

Terahertz (THz) waves^{1,2} have attracted increasing attention because of their unique properties. Many THz-wave applications have been proposed in a wide variety of fields such as spectroscopy,^{3,4} biomedicine,⁵ telecommunication,⁶ and imaging.^{7,8}

To date, a number of techniques for generating THz waves have been reported, including solid state devices,^{9,10} nonlinear optical crystals,¹¹ air plasma,¹² frequency combs,¹³ and photoconductive antennae (PCA).^{14,15} Among these THz generation techniques, continuous-wave (cw) generation of THz waves by PCA-based photomixers has recently emerged as a unique THz source.¹⁶ Photomixing of two-colored cw lasers induces amplitude modulation of the photocurrent through the gap, and this beat signal, whose frequency is in the THz range, generates continuous THz waves. This photomixing technique has a higher spectrum resolution in the frequency domain and is more suitable for spectroscopy. Indeed, Roggenbuck *et al.*¹⁷ reported versatile applications of the cw photomixing technique to the spectroscopy of solid-state samples.

As another application of the cw THz source, electron paramagnetic resonance (EPR) spectroscopy in the THz region is promising. EPR is a unique characterization technique used in many research fields, including chemistry, biology, and engineering.¹⁸ It will make it

possible to obtain microscopic insights into sample properties using electron spins as a probe.

Commercial EPR spectrometers are usually operated in the microwave region, but its frequency extension to the THz region produces several unique advantages.^{19–22} First, the sensitivity increases as the Zeeman splitting is increased. Second, field-dependent interactions (e.g., the anisotropic Zeeman interaction) can be better resolved. Third, spin systems with large zero-field splitting (ZFS) are EPR-silent or difficult to detect at low frequencies, but can be detected by using THz waves, whose energy is comparable to ZFS. In addition, multi-frequency EPR measurement allows the spectroscopic investigation of spin-related phenomena.^{23,24}

In THz EPR experiments, backward traveling-wave oscillators (BWOs) or solid-state multiplier chains are used as the THz source, while liquid-helium-cooled bolometers are often used as the detector. However, these combinations require considerable space, operator experience, and cost. In addition, BWOs are quasi-tunable cw oscillators in that the output power is strongly frequency-dependent.

In this article, we report a unique application of PCA-based cw photomixers to electron paramagnetic resonance (EPR) spectroscopy in the THz region. The developed technique possesses high spectral

resolution in the frequency domain, typically better than 10 MHz, and continuously frequency-tunable in a wide frequency range, thus enabling seamless EPR spectroscopy of versatile samples in the THz region.

Figure 1(a) shows the experimental setup for EPR spectroscopy. Two InGaAs PCAs (emitter and receiver) purchased from TOPTICA²⁵ were used for cw THz generation/detection in this study. Two distributed-feedback (DFB) lasers operating at around 1550 nm (f_1 and f_2) were used to generate THz waves ($f_1 - f_2 = f_{\text{THz}}$) by photo-mixing.²⁶ In our setup, THz waves in the range of 0.05–1.1 THz could be generated by sweeping the laser frequency, and the frequency resolution of the emitted THz wave was better than 10 MHz (mostly determined by the stability of DFB lasers). The typical output power of the source was several tens of μW at 0.05 THz and rapidly decreased to less than 1 μW at 0.5 THz. Since bow-tie antennae were used in this study, the polarization direction of the emitter and receiver was adjusted to coincide beforehand.

THz waves were collimated and focused with two plano-convex lenses made of polymethylpentene (TPX).²⁷ A pellet-shaped sample was mounted on a polyethylene sheet and placed at the focusing point of the THz waves. The beam waist at 0.3 THz was typically 0.8 mm in this setup. All optical components, including two PCAs, lenses, and a sample holder, were packaged into a compact optical cage, and the whole assembly was inserted at the center of a cryogen-free

superconducting magnet, as shown in Fig. 1(b). We note that THz generation/detection by PCA is superior to other THz-EPR setups, since PCA devices are largely unaffected by the magnetic field.²⁸ Indeed, the conventional light source and detector have to be placed away from the magnet center to avoid possible influences due to the stray magnetic field.

By adopting the transmission-type setup rather than the cavity setup, multi-frequency measurement becomes possible. The emitter PCA generated linearly polarized THz waves, which can be expressed by a linear combination of right- and left-circularly polarized electromagnetic waves. At the EPR transition, a left-circularly polarized wave is selectively absorbed by electron spins [Fig. 1(c)], and hence the linearly polarized THz waves are converted to the elliptically polarized waves detected by the receiver PCA. The photocurrent flowing in the receiver PCA is given by $I_{\text{ph}} \propto E_{\text{THz}} \cos(2\pi\Delta L f_{\text{THz}}/c)$, where E_{THz} is the amplitude of the terahertz electric field, ΔL is a difference in the optical path length, and c is the speed of light. ΔL is given by $\Delta L = L_{\text{emitter}} + L_{\text{THz}} - L_{\text{receiver}}$, where L_{emitter} and L_{receiver} are the optical path length from the laser to the emitter and receiver, respectively, and L_{THz} is the length between the emitter and receiver, including the sample thickness. Therefore, it was found that interference fringes appeared when f_{THz} was swept. In this study, we first tuned f_{THz} so that the photocurrent showed the local maximum of a fringe and monitored it while a magnetic field was swept. Then, EPR signals were detected as a decrease in the photocurrent when the EPR resonance condition was satisfied.

In order to increase the sensitivity, THz waves were amplitude-modulated at several kHz by changing the bias voltage of the emitter PCA and demodulated at the receiver PCA using a lock-in amplifier. The dynamic range of this system was typically around 90 dB with a time constant of 300 ms. The room-temperature sample bore was 100 mm in diameter. All measurements were carried out at room temperature.

The inset of Fig. 2 shows a typical EPR spectrum of a 2,2-diphenyl-1-picrylhydrazyl (DPPH) radical observed at $f_{\text{THz}} = 0.1606$ THz. DPPH is known as an EPR standard sample and exhibits a temperature-independent g value ($g = 2.0036$).²⁹ The sample was a pellet-shaped powder with a diameter of 10 mm and a thickness of about 0.5 mm. It is clearly observed that the transmitted intensity sharply decreased at 5.694 T. We carried out similar measurements at more than 20 frequencies and confirmed that the resonance field shifted linearly with THz frequency, as shown in Fig. 2. The resonance condition of EPR absorption is theoretically given by $h\nu = g\mu_B B$,¹⁸ where h is the Planck constant, ν is the frequency, g is the g value, μ_B is the Bohr magneton, and B is magnetic flux density. Therefore, the observed signal was in good agreement with the expected behavior of EPR. The slope of the fitted straight line corresponds to the g value, which is a material-dependent parameter. The upper frequency was 0.27 THz in this setup but was merely limited by the maximum field of the magnet. Therefore, in principle, there is no experimental constraint in the frequency range.

The observed linewidth was about 1 mT in the frequency region up to 0.1 THz but gradually increased to 1.5 mT as the frequency increased to 0.26 THz. These values were larger than that of typical EPR spectra in the microwave range. The origin could be attributed to the g -value anisotropy, which was apparent in the THz region.³⁰ The observed single absorption line can be used as an EPR standard in the

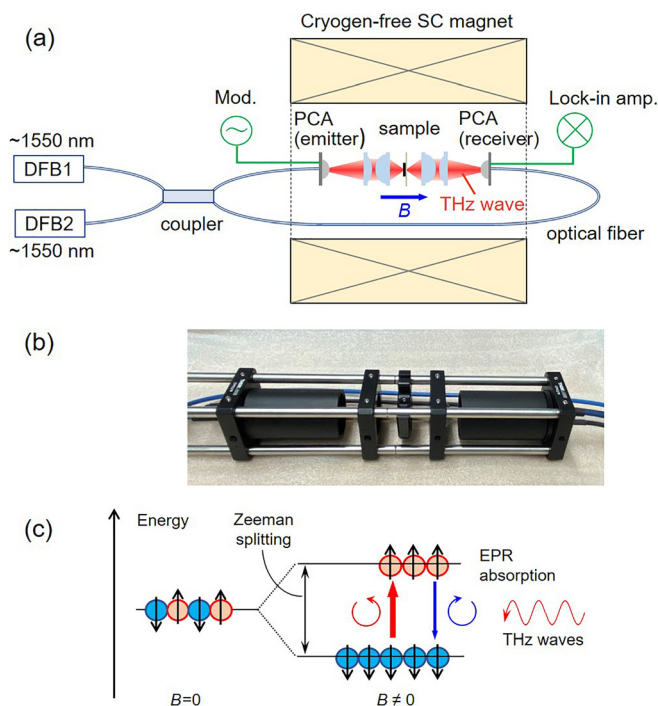


FIG. 1. (a) Experimental setup of EPR spectroscopy using a cw tunable THz generation/detection system. (b) The assembly of the emitter and receiver PCA, lenses, and a sample holder. (c) The principle of EPR absorption. The energy level for $S = 1/2$, which is degenerated at zero field, is split into two Zeeman levels in the presence of the magnetic field. Because of the population difference between $S_z = \pm 1/2$ levels, a net absorption at the EPR transition was given by the left-circularly polarized component upon EPR transition.

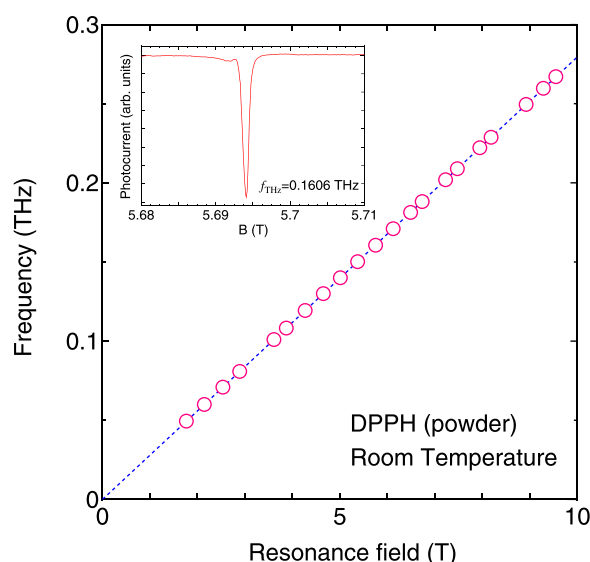


FIG. 2. Resonance field vs frequency derived from multi-frequency EPR measurements of a powder sample of DPPH radical. The g value can be obtained from the slope of a fitted straight line. The inset shows the raw EPR spectrum for $f_{\text{THz}} = 0.1606$ THz at room temperature.

THz region, though it was reported that the linewidth substantially depended on sample batch and solvent from which DPPH was crystallized.³¹

From the signal-to-noise ratio and sample mass, we estimated the minimum detectable spin number N_{min} at room temperature as $N_{\text{min}} \sim 1 \times 10^{16}$ spins. The detection sensitivity was defined by N_{min} divided by the linewidth and estimated as 4×10^{15} spins/mT in the present case. The former refers to the total spin numbers necessary for EPR detection of a specific sample, while the latter refers to the sensitivity inherent in the apparatus.

In order to demonstrate high spectral resolution, a single crystal of copper sulfate ($\text{CuSO}_4 \cdot 5\text{H}_2\text{O}$) was measured at different THz frequencies. The sample was a blue-colored, plate-like crystal mounted on a polyethylene sheet so that the magnetic field was perpendicular to the plane. In this compound, a divalent copper ion (Cu^{2+}) is EPR-active ($3d^9$, $S = 1/2$) and located at the center of a distorted octahedron.³² Since there are two inequivalent copper sites in the crystal, we expected two EPR absorptions in the field-sweep data. However, in the microwave region, these two EPR signals were merged into one EPR spectrum, due to the exchange interaction between the two copper sites.

Figure 3 shows the EPR signal of $\text{CuSO}_4 \cdot 5\text{H}_2\text{O}$ in the units of the g value, where a magnetic field was converted to the g value according to $g = h\nu/\mu_B B$. This plot simplifies the comparison of data observed in different field ranges. In the data at $f_{\text{THz}} = 0.2460$ THz, a clear splitting of the EPR signal was visible, as expected. As shown in the inset, these two absorptions obeyed the linear relationship. Note that the splitting is negligibly small in the microwave region but becomes wider as the THz frequency increases. The g values were $g_1 = 2.083$ and $g_2 = 2.311$, which were in agreement with previous research.^{33,34}

There are few reports of the application of PCA to EPR measurements, except for the work by Kozuki *et al.*³⁵ Their setup was similar to those of THz time-domain spectroscopy (TDS), and the transmitted

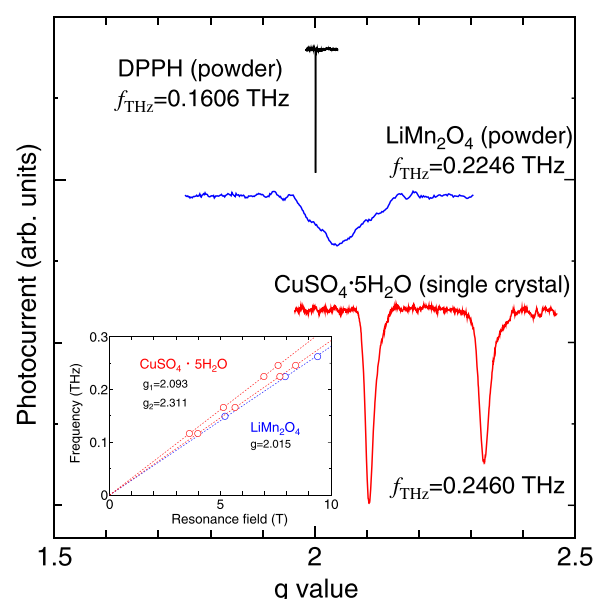


FIG. 3. Room-temperature EPR spectra for DPPH powder, LiMn_2O_4 powder, and single-crystalline $\text{CuSO}_4 \cdot 5\text{H}_2\text{O}$ shown in the units of the g value. The inset shows resonance field vs frequency for LiMn_2O_4 and $\text{CuSO}_4 \cdot 5\text{H}_2\text{O}$, obtained from multi-frequency EPR measurements. Dotted lines are the fitted results assuming the EPR resonance condition.

intensity through the sample placed in a static magnetic field was measured by the cross-polarization configuration to increase the sensitivity. EPR signals in the frequency domain were obtained by Fourier-transformation of THz pulses. They observed EPR signals of $\text{CuSO}_4 \cdot 5\text{H}_2\text{O}$ at different applied magnetic fields, but the spectral resolution was 1.25 GHz, two orders of magnitude worse than our setup. In addition, the signal-to-noise ratio was insufficiently low, compared to the present work.

Taking advantage of the high spectral resolution, applications to transition metal compounds will be promising. This is because these compounds often exhibit rather broad EPR spectra due to strong magnetic interactions, which makes EPR detection quite difficult by the standard EPR spectrometers. As one of such candidates, lithium-containing transition metal compounds are proposed. In recent years, the search for superior electrode materials to be used in the development of lithium ion batteries (LIBs)^{36–38} has become important for improving LIB performance. Many types of lithium-containing transition metal compounds have been tested.^{39,40} However, fundamental magnetic properties such as the g value remain unknown in these compounds. Therefore, EPR measurements would be useful to determine g values, hyperfine and exchange interactions, and zero-field splitting, which are sensitive to their valence state and their local coordination environment. In this sense, our system is simple but useful for investigating these systems in a spectroscopic manner.

Here, we show THz EPR results for lithium manganese oxide, LiMn_2O_4 ,⁴¹ as a practical example. This compound is well known as a positive-electrode material for LIB,⁴² and undergoes antiferromagnetic transition at low temperature.⁴¹ The sample was purchased from Sigma Aldrich and used as received. As shown in Fig. 3, a broad and single EPR absorption was observed at around $g = 2.01$ at room

temperature. A more precise g value was $g = 2.015$, as determined by multi-frequency EPR and shown in the inset of Fig. 3. The linewidth of LiMn_2O_4 was greater than 1 T for $f_{\text{THz}} = 0.2246$ THz; hence, THz waves were indispensable for detecting EPR signals in this compound. In the present setup, we measured a pristine sample where the valence of the manganese ion was $\text{Mn}^{+3.5}$. It is expected that the valence may be changed during the charge/discharge process, which would substantially affect the EPR spectra. Thus, operando EPR^{43,44} (*in situ* EPR of devices in operation) of LIB-related materials in the THz region would be a promising application in the future.

In the present setup, the magnetic field was swept at a fixed frequency to measure EPR spectra, but frequency-sweep measurements at a constant magnetic field using the chosen emitter/receiver are another option. Since frequency sweeps can be performed much faster than field sweeps, this modality may potentially lead to strongly reduced measurement times. In our setup, the maximum frequency sweep rate was 0.1 THz/s, which was limited by the response time of temperature control of the laser module. When the frequency is swept, however, the photocurrent oscillates due to the interference fringes between the emitter and receiver branches, and envelope detection of the fringes is needed to obtain EPR spectra. For this purpose, a fiber stretcher was used as a phase modulator for envelope detection.⁴⁵

In the context of high-frequency EPR, multi-frequency EPR (MFEPR),^{23,24} frequency-domain EPR (FDEPR),^{46,47} and Fourier-transform EPR (FTEPR)⁴⁸ in the THz region are compared. MFEPR and FDEPR combine a relatively high sensitivity with a high spectral resolution and cover a wide frequency range up to 1 THz, though multiple light sources (typically, backward travelling-wave oscillator or solid-state multiplier chain) are needed to cover the entire range. FTEPR can be performed in a broad frequency region between 0.1 and 5 THz, though the sensitivity and spectral resolution (~ 300 MHz) are worse than those of other EPR techniques. Between 0.1 and 0.4 THz, the coherent synchrotron radiation source works best among the available light sources. The PCA-based technique has a high spectral resolution (~ 10 MHz) and covers a wide frequency region up to 1.1 THz using a single emitter (up to 2.7 THz with an additional laser⁴⁹). The sensitivity is currently worse than that of MFEPR and FDEPR, but would be improved with developments of PCA devices. A unique advantage of the PCA-based technique is the compact setup in which the source and detector are incorporated together.

In summary, we developed a unique EPR spectroscopy technique in the THz region using a cw THz generation/detection system based on PCA photomixers. This frequency-tunable source enabled seamless EPR spectroscopy in the frequency range of 0.05–0.3 THz. This upper limit was merely set by the available magnetic field, and in the future, EPR measurement in the higher frequency region will be possible. We observed room-temperature EPR absorptions of transition metal compounds, in addition to a DPPH radical, and demonstrated high spectral resolution for samples with broad EPR spectra. In addition, all components including the emitter and receiver PCA can be assembled in the magnet bore, making the experimental setup compact and simple. In principle, our technique can be applied to other commercial PCA systems (e.g., verTera system supplied by Bruker⁵⁰) and will offer good opportunities for detailed EPR analysis in the THz region.

We thank S. Okubo for supplying single crystals of copper sulfate and for useful discussions. This work was supported by

Competitive Funding Programs “Collaborative Research Based on Industrial Demand” from Japan Science and Technology Agency (No. JPMJSK1615).

REFERENCES

- M. Mittleman, *J. Appl. Phys.* **122**, 230901 (2017).
- S. S. Dhillon, M. S. Vitiello, E. H. Linfield, A. G. Davies, M. C. Hoffmann, J. Booske, C. Paoloni, M. Gensch, P. Weightman, G. P. Williams, E. Castro-Camus, D. R. S. Cumming, F. Simoons, I. Escorcia-Carranza, J. Grant, S. Lucyszyn, M. Kuwata-Gonokami, K. Konishi, M. Koch, C. A. Schmuttermaier, T. L. Cocker, R. Huber, A. G. Markelz, Z. D. Taylor, V. P. Wallace, J. A. Zeitler, J. Sibik, T. M. Korter, B. Ellison, S. Rea, P. Goldsmith, K. B. Cooper, R. Appleby, D. Pardo, P. G. Huggard, V. Krozer, H. Shams, M. Fice, C. Renaud, A. Seeds, A. Stöhr, M. Naftaly, N. Ridler, R. Clarke, J. E. Cunningham, and M. B. Johnston, *J. Phys. D* **50**, 043001 (2017).
- M. Hangyo, M. Tani, and T. Nagashima, *Int. J. Infrared Millimeter Waves* **26**, 1661 (2005).
- N. J. J. van Hoof, S. E. T. ter Huurne, J. Gómez Rivas, and A. Halpin, *Opt. Exp.* **26**, 32118 (2018).
- L. Yu, L. Hao, T. Meiqiong, H. Jiaoqi, L. Wei, D. Jinying, C. Xueping, F. Weiling, and Z. Yang, *RSC Adv.* **9**, 9354 (2019).
- T. Nagatsuma, G. Ducournau, and C. C. Renaud, *Nat. Photonics* **10**, 371 (2016).
- N. Rotenberg and L. Kuipers, *Nat. Photonics* **8**, 919 (2014).
- D. M. Mittleman, *Opt. Express* **26**, 9417 (2018).
- B. S. Williams, *Nat. Photonics* **1**, 517 (2007).
- K. Sengupta, T. Nagatsuma, and D. M. Mittleman, *Nat. Electron.* **1**, 622 (2018).
- K. Kawase, J. Shikata, and H. Ito, *J. Phys. D* **34**, R1 (2001).
- J. Dai, J. Liu, and X.-C. Zhang, *IEEE J. Sel. Top. Quant. Electron.* **17**, 183 (2011).
- D. Burghoff, T.-Y. Kao, N. Han, C. W. I. Chan, X. Cai, Y. Yang, D. J. Hayton, J.-R. Gao, J. L. Reno, and Q. Hu, *Nat. Photonics* **8**, 462 (2014).
- M. Tani, M. Herrmann, and K. Sakai, *Meas. Sci. Technol.* **13**, 1739 (2002).
- N. M. Burford and M. O. El-Shenawee, *Opt. Eng.* **56**, 010901 (2017).
- S. Preu, G. H. Döhler, S. Malzer, L. J. Wang, and A. C. Gossard, *J. Appl. Phys.* **109**, 061301 (2011).
- A. Roggenbuck, H. Schmitz, A. Deninger, I. C. Mayorga, J. Hemberger, R. Güsten, and M. Grüninger, *New J. Phys.* **12**, 043017 (2010).
- Electron Paramagnetic Resonance of Transition Ions*, edited by A. Abragam and B. Bleaney (Clarendon Press, Oxford, 1970).
- H. Ohta, S. Okubo, K. Kawakami, D. Fukuoka, Y. Inagaki, T. Kunitomo, and Z. Hiroi, *J. Phys. Soc. Jpn.* **72**, Suppl. B 26 (2003).
- N. Nakagawa, T. Yamada, K. Akioka, S. Okubo, S. Kimura, and H. Ohta, *Int. J. Infrared Millimeter Waves* **19**, 167 (1998).
- J. Krzystek, A. Ozarowski, and J. Telser, *Coord. Chem. Rev.* **250**, 2308 (2006).
- E. J. Reijerse, *Appl. Mag. Reson.* **37**, 795 (2010).
- J. Telser, J. Krzystek, and A. Ozarowski, *J. Biol. Inorg. Chem.* **19**, 297 (2014).
- T. Okamoto, E. Ohmichi, S. Okubo, and H. Ohta, *J. Phys. Soc. Jpn.* **87**, 013702 (2018).
- See <https://www.toptica.com/> for “TOPTICA Photonics AG.”
- Y.-S. Lee, *Principles of Terahertz Science and Technology* (Springer, Berlin, 2009). Chap. 4.
- See <https://www.batop.de/> for “BATOP GmbH.”
- S. A. Crooker, *Rev. Sci. Instrum.* **73**, 3258 (2002).
- N. D. Yordanov, *Appl. Mag. Reson.* **10**, 339 (1996).
- T. Tatsukawa, T. Maeda, H. Sasai, T. Idehara, M. Mekata, T. Saito, and T. Kanemaki, *Inter. J. Infrared Millimeter Waves* **16**, 293 (1995).
- J. Krzystek, A. Sienkiewicz, L. Pardi, and L. C. Brunel, *J. Mag. Reson.* **125**, 207 (1997).
- C. A. Beevers and H. Lipson, *Proc. R. Soc. London, Ser. A* **146**, 570 (1934).
- D. M. S. Bagguley and J. H. E. Griffiths, *Proc. R. Soc. London, Ser. A* **201**, 366 (1950).
- K. Ono and M. Ohtsuka, *J. Phys. Soc. Jpn.* **13**, 206 (1958).
- K. Kozuki, T. Nagashima, and M. Hangyo, *Opt. Express* **19**, 24950 (2011).
- V. Etacheri, R. Marom, R. Elazari, G. Salitra, and D. Aurbach, *Energy Environ. Sci.* **4**, 3243 (2011).

- ³⁷L. Lu, X. Han, J. Li, J. Hua, and M. Ouyang, *J. Power Sources* **226**, 272 (2013).
- ³⁸M. Li, J. Lu, Z. Chen, and K. Amine, *Adv. Mater.* **30**, 1800561 (2018).
- ³⁹J. Lu, Z. Chen, F. Pan, Y. Cui, and K. Amine, *Electrochem. Energy Rev.* **1**, 35 (2018).
- ⁴⁰M. S. Whittingham, *Chem. Rev.* **104**, 4271 (2004).
- ⁴¹S. Takano, T. Kaji, S. Okubo, M. Yoshida, Y. Inagaki, S. Kimura, T. Asano, H. Ohta, T. Kunimoto, R. Dziembaj, M. Molenda, and C. Rudowicz, *Phys. Stat. Sol. C* **3**, 2820 (2006).
- ⁴²K. M. Shaju and P. G. Bruce, *Chem. Mater.* **20**, 5557 (2008).
- ⁴³M. Sathiy, J.-B. Leriche, E. Salager, D. Gourier, J.-M. Tarascon, and H. Vezin, *Nat. Commun.* **6**, 6276 (2015).
- ⁴⁴M. Tang, A. Dalzini, X. Li, X. Feng, P.-H. Chien, L. Song, and Y.-Y. Hu, *J. Phys. Chem. Lett.* **8**, 4009 (2017).
- ⁴⁵A. Roggenbuck, K. Thirunavukkuarasu, H. Schmitz, J. Marx, A. Deninger, I. C. Mayorga, R. Güsten, J. Hemberger, and M. Grüninger, *J. Opt. Soc. Am. B* **29**, 614 (2012).
- ⁴⁶O. Laguta, M. Tucek, J. van Slageren, and P. Neugebauer, *J. Magn. Reson.* **296**, 138 (2018).
- ⁴⁷J. van Slageren, S. Vongtragool, B. Gorshunov, A. A. Mukhin, N. Karl, J. Krzystek, J. Telser, A. Müller, C. Sangregorio, D. Gatteschi, and M. Dressel, *Phys. Chem. Chem. Phys.* **5**, 3837 (2003).
- ⁴⁸J. Nehr Korn, K. Holldack, R. Bittl, and A. Schnegg, *J. Magn. Reson.* **280**, 10 (2017).
- ⁴⁹A. Deninger, A. Roggenbuck, S. Schindler, and S. Preu, *J. Infrared Millimeter Terahertz Waves* **36**, 269 (2015).
- ⁵⁰See <https://www.bruker.com/> for “Bruker Corporation.”